

Cite this: *Soft Matter*, 2012, **8**, 1521

www.rsc.org/softmatter

PAPER

## Phase diagram of two-dimensional systems of dipole-like colloids

Heiko Schmidle,<sup>\*a</sup> Carol K. Hall,<sup>b</sup> Orlin D. Velev<sup>b</sup> and Sabine H. L. Klapp<sup>a</sup>

Received 18th August 2011, Accepted 3rd November 2011

DOI: 10.1039/c1sm06576a

Based on Discontinuous Molecular Dynamics (DMD) simulations we present a phase diagram of two-dimensional nano-particles with dipole-like short-ranged interactions. Similar to systems with true, long-ranged dipolar interactions the present system undergoes a transition from an isotropic fluid phase into a polymer-like fluid, characterized by an association of most particles into clusters. Further decrease of the temperature leads to a percolated system which, moreover, displays dynamical properties reminiscent of a gel. Specifically, we find a plateau in the mean-squared displacement and a non-gaussian behavior of the self-part of the van Hove correlation function. In the high density region we observe crystallization from the isotropic fluid into a solid phase with hexagonal order. Surprisingly, the crystallization is accompanied by a global parallel ordering of the dipole moments, *i.e.*, a ferroelectric phase. This behavior is in marked contrast to what is found in 2D systems with long-ranged dipolar interactions. Our results allow insights into the design of gel-like or highly ordered structures at interfaces, shells around droplets and bubbles and new-sheet like materials.

### 1 Introduction

The self-assembly of colloidal particles with anisotropic interactions is a rapidly expanding research field.<sup>1,2</sup> “Classical” realizations of such systems are (para- or ferro)magnetic nanoparticles with and without magnetic fields, as well as polarizable colloids in electric fields. In both cases, the dominant interactions are dipolar in character. Another example is the broad class of so-called “patchy” colloids consisting of nanoparticles with adhesive functional molecular groups,<sup>3,4</sup> which yield short-ranged directional interactions (such as, *e.g.*, proteins<sup>5</sup>). Moreover, within the last few years there has been significant progress in the synthesis of “Janus”-like particles consisting of two hemispheres with different physical or chemical properties.<sup>6–8</sup> Understanding the complex, self-assembled structures formed by such anisotropic particles<sup>9</sup> and the manipulation of these structures by external fields (and other factors such as chemical composition and thermodynamic parameters) is important *e.g.*, for the development of new, “smart” or “stimuli-responsive”, materials,<sup>2</sup> but also for the advancement of devices such as sensors and nano-robots.<sup>10–12</sup>

From the theoretical perspective, model systems composed of dipolar or patchy particles have been extensively studied both by computer simulations (see *e.g.* ref. 4, 13–17) and by (semi-) analytical approaches (see *e.g.* ref. 18–20). One focus is the equilibrium self-assembly phenomena such as the (reversible)

formation of strings, rings, and percolated networks, as well as of (possibly anisotropic) high-density phases. In addition, particular interest has been recently devoted to dynamic phenomena such as gelation and structural arrest.<sup>21</sup> Indeed, while most of the above-mentioned models exhibit large and even percolated clusters at sufficiently low densities and sufficient strengths of anisotropic interactions, anomalous dynamic behavior characteristic of gelation only occurs in specific systems.<sup>17</sup> An example of a dipolar system exhibiting (reversible) gelation is a fluid of dumbbells which consists of a positively and negatively charged sphere.<sup>22</sup> On the other hand, to our knowledge, no gel-like dynamics has so far been reported for systems of dipolar hard spheres (DHS) and dipolar soft spheres (DSS).

In the present study we explore by computer simulations the self-assembly and phase behavior of a two-dimensional (2D) system of colloidal particles with modified dipolar interactions. Specifically, we consider a model which was recently proposed in ref. 23 to simulate dipole-like systems *via* the so-called Discontinuous Molecular Dynamics (DMD) method,<sup>23–25</sup> a special form of (event-driven) MD. In this context, the true, continuous, long-range dipolar potential is approximated by a discontinuous, three-step potential which (roughly) preserves the directional dependence of the original interaction, particularly the preference of head-tail-arrangements, but restricts its range. The resulting model may be seen as some sort of screened dipolar system; in fact, in systems of polarizable colloids such a screening induced by charges in the solvent is certainly realistic. Experimental examples of such systems are reported in ref. 26 and 27. In these studies induced dipolar particles are generated *via* applying an AC electric field to dielectric particles. The particles are suspended in water, yielding a pronounced screening which can be

<sup>a</sup>Institute of Theoretical Physics, Technical University Berlin, Hardenbergstr. 36, 10623 Berlin, Germany. E-mail: schmidle@physik.tu-berlin.de

<sup>b</sup>Department of Chemical and Biomolecular Engineering, North Carolina State University, Raleigh, North Carolina, 27695-7905, USA

adjusted through the pH of the solvent. More generally, our model may be considered as a simple representative of a networking-forming system, the big advantage being that it is computationally much less costly than corresponding models with true electrostatic interactions. Indeed, investigating this model in a three-dimensional (3D) set-up for a wide range of parameters,<sup>23</sup> a variety of complex (aggregated or positionally ordered) states can be observed, and an even broader variety is found in corresponding two-component systems.<sup>28</sup>

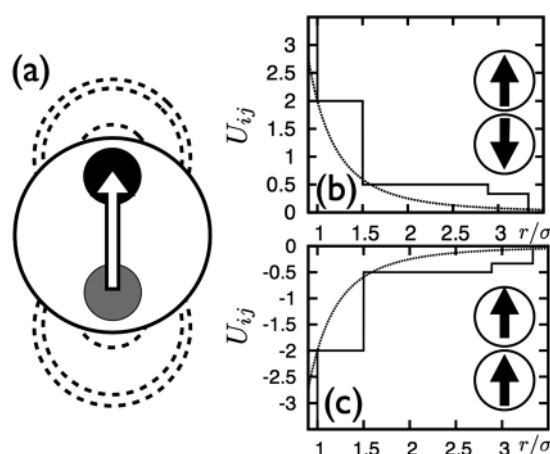
Here we investigate the (one-component) model of ref. 23 in 2D, focussing on both, static and dynamic phenomena. Our motivation to explore in more detail to the 2D situation is driven, on one hand, by the fact that many experiments involving self-assembling colloids are actually done at surfaces and/or in thin films.<sup>11,29–31</sup> Moreover, from a conceptual point of view, research on true dipolar systems has revealed that the spatial dimension of the system strongly affects the (equilibrium) behavior; examples being the absence of spontaneous, global polarization at high densities in 2D,<sup>18,32,33</sup> the preference of rings (relative to chains) at low densities,<sup>15</sup> and the confinement-induced shift of the vapor–liquid coexistence curves in dipolar systems with additional van der Waals interactions.<sup>34</sup> We investigate the model system through a number of order parameters. Based on these quantitative measures, we are able to map out a sketch of a phase diagram involving an isotropic fluid, a polymerized fluid, a percolated gel, and a hexagonal crystal. Most notably, we show that the dynamics in percolated phase has gel-like features. Moreover, the crystalline phase is not only translationally ordered, but also of ferroelectric orientation.

The rest of the paper is organized as follows. In Sec.2 we describe our model and give some details of the DMD simulations. Numerical results are presented and discussed in Sec. 3, where we first consider (in Sec. 3.1) the low-density states and corresponding dynamic properties. Section 3.2 is then devoted to the ordering phenomena observed at high densities. Finally, in Sec. 4 we summarize our results and present a brief outlook of possible future work.

## 2 Model and simulation method

In the present study we employ the DMD simulation technique.<sup>23–25</sup> This method is a fast alternative to traditional Molecular Dynamics (MD) simulations, where the forces on the particles are computed in each (constant) time step. In DMD, on the contrary, we compute the forces only when two particles collide. By solving the corresponding (Newton) equations of motion we can then advance the positions and velocities of all particles until the next collision occurs. In between two collisions the particles move ballistically. Thus we significantly reduce the amount of force computations and thereby save computational time. In our earlier work<sup>34</sup> we performed extensive Monte Carlo simulations with true dipoles. The long-range interactions were handled *via* the Ewald summation. The gain in simulation time of the DMD method compared to the long-range interactions is about 10–20 times faster. Before we go into some technical details of the simulation method we describe the pair interactions between particles.

We model each dipole-like colloid by two oppositely “charged” particles embedded in a hard sphere (HS). In Fig. 1(a)



**Fig. 1** Schematic representation of our model. The dipole-like colloids are represented by two oppositely charged spheres (shown by black and grey) embedded into a hard sphere. The dashed lines indicate the potential steps. In (b) and (c) we plot the total interaction potential ( $U_{ij}$  in units of  $\mu^2/\sigma^3$ ) on the y-axis and the distance ( $r/\sigma$ ) on the x-axis, related to the most repulsive and attractive configurations of two particles [see cartoons in (b) and (c)]. The dashed lines indicate the corresponding potentials for true dipoles.

we show a schematic representation of our model. Like charges repel one another by a three-step square-shoulder potential ( $U_{SS}$ ), and unlike charges interact *via* an attractive three-step square-well potential ( $U_{SW}$ ). The HS potential is defined as

$$U_{HS}(r_1) = \begin{cases} \infty, & \text{if } r_1 < \sigma \\ 0, & \text{if } r_1 > \sigma, \end{cases} \quad (1)$$

where  $r_1$  is the distance between two HS and  $\sigma$  is the HS diameter. Further, the “charge–charge” interactions are defined by

$$U_{SS}(r_2) = \begin{cases} \infty, & \text{if } r_2 < \sigma_1 \\ \varepsilon_1, & \text{if } \sigma_1 < r_2 < (1 + \lambda_1)\sigma_1 \\ \varepsilon_2, & \text{if } (1 + \lambda_1)\sigma_1 < r_2 < (1 + \lambda_2)\sigma_1 \\ \varepsilon_3, & \text{if } \sigma_2 < r_2 < (1 + \lambda_3)\sigma_1 \\ 0, & \text{if } r_2 > (1 + \lambda_3)\sigma_1 \end{cases} \quad (2)$$

and

$$U_{SW}(r_2) = \begin{cases} \infty, & \text{if } r_2 < \sigma_1 \\ -\varepsilon_1, & \text{if } \sigma_1 < r_2 < (1 + \lambda_1)\sigma_1 \\ -\varepsilon_2, & \text{if } (1 + \lambda_1)\sigma_1 < r_2 < (1 + \lambda_2)\sigma_1 \\ -\varepsilon_3, & \text{if } \sigma_2 < r_2 < (1 + \lambda_3)\sigma_1 \\ 0, & \text{if } r_2 > (1 + \lambda_3)\sigma_1. \end{cases} \quad (3)$$

In eqn (2) and (3),  $r_2$  is the distance between two embedded charges of different HS particles. The charged particles have a diameter  $\sigma_1 = 0.3\sigma$ . The potential steps are defined by their magnitudes  $\varepsilon_1$ ,  $\varepsilon_2$ , and  $\varepsilon_3$ , respectively, and the step widths are  $\lambda_1$ ,  $\lambda_2$ , and  $\lambda_3$ . To define the actual values of these parameters we first need to introduce reduced units. We define a reference interaction strength by  $\varepsilon^* = \mu^2/\sigma^3$ , where  $\mu$  is the target dipole moment we aim to model. Dimensionless potential steps are then defined by  $\varepsilon_\alpha = \varepsilon_\alpha/\varepsilon^*$ , where  $\alpha = 1, 2, 3$ . Further, the reduced temperature

is given by  $T^* = k_B T / \varepsilon^*$ , where  $k_B$  is the Boltzmann constant and  $T$  is the temperature. We reduce the density in the standard way by  $\rho^* = N\sigma^2/A$ , where  $A$  is the area of the simulation box. The time in the simulations is also reduced by  $t^* = t/\sqrt{\sigma^2(k_B T/m)}$ , where  $m$  is the mass of the particles.

The parameters appearing in eqn (2) and (3) are chosen in such a way that the resulting total potential matches, as far as possible, the full dipole–dipole interaction  $U_{DD}(r_{ij}) = (1/r_{ij}^3)[\boldsymbol{\mu}_i \cdot \boldsymbol{\mu}_j - (3/r_{ij}^2)(\boldsymbol{\mu}_i \cdot \mathbf{r}_{ij})(\boldsymbol{\mu}_j \cdot \mathbf{r}_{ij})]$ . Specifically, following an earlier DMD study on dipolar-like colloids in three dimensions,<sup>23</sup> we choose  $\lambda_1 = 0.500$ ,  $\lambda_2 = 1.887$  and  $\lambda_3 = 2.333$ . The potential depths are  $\varepsilon_1^* = 2.000$ ,  $\varepsilon_2^* = 1.500$  and  $\varepsilon_3^* = 0.500$ . The resulting total potential for two relevant configurations is plotted in Fig. 1(b) and (c). To locate the embedded charges within the hard spheres, we use the method proposed in ref. 35. Both charges within the particle are bound to the sphere but their distance (in units of  $\sigma$ ) is allowed to move between  $(1 \pm \delta/2)$ .<sup>36</sup> By this choice it is guaranteed that the dipole vector always points through the center of the nano-particles while some fluctuations in its length are allowed. In our simulations we set  $\delta = 0.04$ . Clearly, our model does not account for the long-range character of the true dipole–dipole interactions; however, it mimics the dipole–dipole interaction locally. This is illustrated in Fig. 2 where we show the pair energies for different configurations according to the true dipole–dipole interaction, on the one hand (middle column), and our model, on the other hand (right column). Within our model, the uncertainty of the energy of the side-by-side configurations results from fluctuations emerging from the parameter  $\delta$ . From Fig. 2 it becomes clear that the head-to-tail configuration is the energetically most favorable one, as it is the case for true dipoles. Side-by-side configurations with parallel (antiparallel) orientations are less unfavorable (favorable) than for the true interaction. A particularly important feature is that our model implies a lower energy for the three-particle configuration shown in the last row of Fig. 2. In the best case, depending on the positions of

the embedded charges, the energetic advantage compared to true dipoles is 1.78 times larger.

In the present study, we employ DMD simulations in the canonical ensemble. To this end we use a stochastic thermostat.<sup>37</sup> This widely used method introduces collisions of the colloids with ghost particles representing the heat bath. The ghost particles stabilize the system at a predefined temperature. Details of the DMD method in the canonical ensemble can be found in ref. 25, 38, 39. Here we consider mainly system sizes of  $N = 576$ , 1024, and 1600 particles. In a typical run we use  $5\text{--}10 \times 10^8$  collisions to equilibrate the system and  $5\text{--}10 \times 10^8$  collisions to extract averages. In the low-temperature regime, longer equilibration times are required due to the aggregation and subsequent network formation of the particles.

## 3 Results and discussion

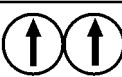
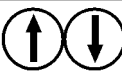
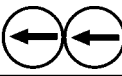

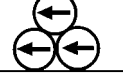
### 3.1 Fluid phases

**3.1.1 Polymerization.** We first study the system at low and medium densities. At high temperatures the colloids form a completely disordered fluid phase corresponding to the behavior of the pure HS system. Upon decreasing the temperature the anisotropic interactions between the dipole-like colloids become more and more important. As a result the particles start to connect into clusters, yielding a polymerization “transition”. In general, there are two different approaches which allow to locate polymerization in the phase diagram. One strategy consists of searching for a maximum in the specific heat.<sup>40</sup> A second technique foots on the so-called degree of polymerization<sup>41,42</sup> defined by

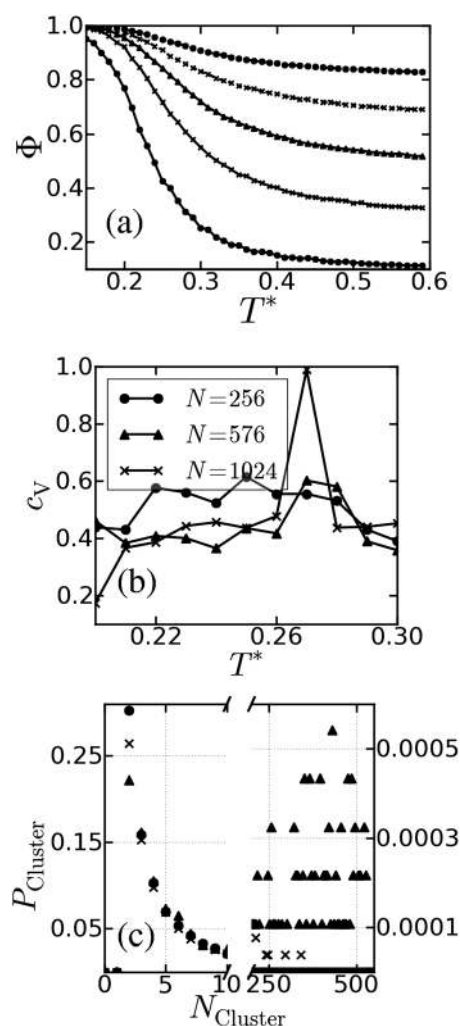
$$\Phi = \left\langle \frac{N_a}{N} \right\rangle. \quad (4)$$

In the above equation,  $N_a$  is the number of particles associated in clusters, and  $N$  is the total number of particles. We consider two particles to be associated into the same cluster if the distance between the HS is smaller than the “critical” radius  $r_c = 1.25\sigma$ . This value was chosen because it corresponds to a distance close to the first minimum of the radial distribution function for a broad range of temperatures and densities. We identify the nearest neighbours by using a Voronoi decomposition. The latter proves to be particularly useful in the high density regime.

In Fig. 3(a) we present results for the two quantities  $\Phi$  and  $c_V$  (inset) as functions of the temperature and different densities. Both quantities have been evaluated for three different system sizes,  $N = 256$ , 576, and  $N = 1024$ . As seen from the inset of Fig. 3(a), the specific heat does display a maximum, but only for the largest system size considered. Moreover, the whole function  $c_V(T^*)$  is subject to strong statistical errors. We therefore focus on the order parameter  $\Phi$ , which turns out to be robust against variation of  $N$ . The polymerization temperature is commonly identified by the inflection point of the function  $\Phi(T^*)$  at a given density.<sup>42</sup> Inspecting the data in Fig. 3(a) one notes that, based on the above criteria, a pronounced transition only occurs at low densities ( $\rho^* < 0.3$ ). Upon increasing  $\rho^*$ , the parameter  $\Phi$  has relatively large, non-zero values already at higher temperatures, making the detection of an inflection point less obvious. Indeed, an inspection of corresponding snapshots from the simulations

Configuration	$U_{ij}$ True Dipoles	$U_{ij}$ DMD Model
	$\frac{\mu^2}{\sigma^3}$	$0 < U_{ij} < \frac{2\mu^2}{3\sigma^3}$
	$-\frac{\mu^2}{\sigma^3}$	$-\frac{2\mu^2}{3\sigma^3} < U_{ij} < 0$
	$-2\frac{\mu^2}{\sigma^3}$	$-2\frac{\mu^2}{\sigma^3}$
	$2\frac{\mu^2}{\sigma^3}$	$2\frac{\mu^2}{\sigma^3}$
	$-\frac{3\mu^2}{2\sigma^3}$	$-\frac{8\mu^2}{3\sigma^3} < U_{ij} < -\frac{4\mu^2}{3\sigma^3}$

**Fig. 2** Interaction energies  $U_{ij}$  for various two-particle configurations, shown in the left column. The middle column gives the energy values according to the true dipole–dipole interaction, while the right column gives the values according to our model. Within the latter, the uncertainty of the energies appearing at the side-by-side configurations arises from the fluctuations of the embedded charges within the HS.



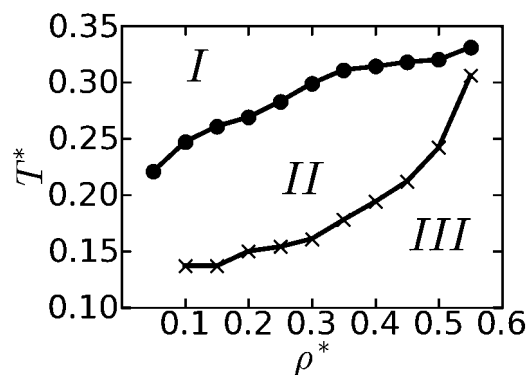
**Fig. 3** (a) Degree of polymerization as function of temperature at different densities. From bottom to top:  $\rho^* = 0.05, 0.15, 0.25, 0.35, 0.55$ . (b) Specific heat  $c_V$  of the system at  $\rho^* = 0.1$  and three system sizes. (c) Probability  $P_{\text{Cluster}}$  of finding a cluster with size  $N_{\text{Cluster}}$  at  $\rho^* = 0.4$  and a system size of  $N = 576$ . Circles correspond to  $T^* = 0.35$ , crosses to  $T^* = 0.25$ , and triangles to  $T^* = 0.2$ . At  $N_{\text{Cluster}} = 2$ , there is a pronounced peak for all three temperatures considered. In the range  $N_{\text{Cluster}} \sim 200$ –576, there is essentially no peak at  $T^* = 0.35$  (circles) and only a small non-zero probability at  $T^* = 0.25$  (crosses). On the other hand, at  $T^* = 0.2$  (triangles) a clear peak arises at  $N_{\text{Cluster}} \sim 400$ .

reveals aggregation into small clusters already at large  $T^*$ . Nevertheless, upon lowering  $T^*$  we observe a change of  $\Phi$  from intermediate values to a value close to 1, indicating a sudden increase of the largest cluster size. As an additional criterion for polymerization particularly at high densities, we have investigated the cluster-size distribution, that is, the probability to find a cluster of size  $N_{\text{Cluster}}$ . In Fig. 3(b) we plot corresponding numerical results for  $\rho^* = 0.4$  and three different temperatures (at the system size  $N = 576$ ). Above the polymerization temperature  $T^* = 0.314$  [as determined *via* the inflection point of the function  $\Phi(T^*)$ ] most particles are already associated into small clusters of size  $2 < N_{\text{Cluster}} < 10$ . Within the polymerized state ( $T^* = 0.25$ ) the distribution reflects the presence of a small number of large clusters with  $N_{\text{Cluster}} \sim 250$  [see crosses on the right hand side of

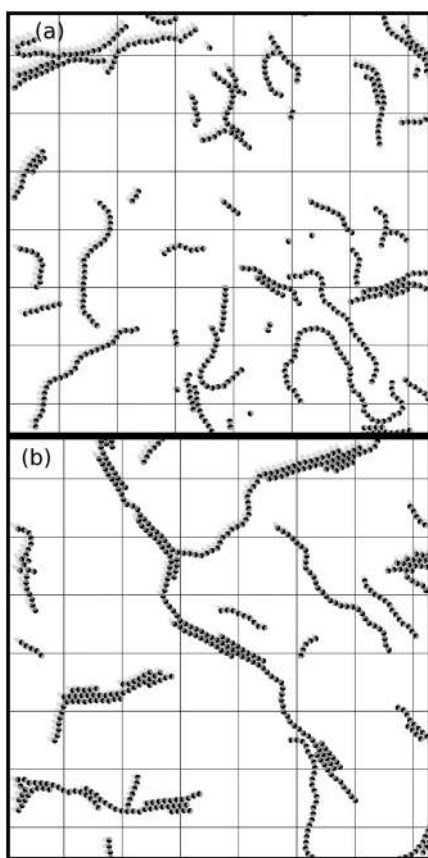
Fig. 3(b)]. By further cooling the system one then observes the emergence of a second peak in the cluster-size distribution, indicating the presence of a significant amount of large clusters. This occurs slightly above the percolation temperature ( $T_{\text{perc}}^* = 0.194$ , see next section). The estimated transition line  $T^*(\rho^*)$  which separates the non-aggregated high-temperature regime (region I) from the aggregated polymerized “state” (region II) is shown in Fig. 4. Interestingly, these predictions from our DMD simulations are quite consistent with those from a recent integral equation study<sup>18</sup> for a two-dimensional system of DHS. In the latter study, the temperatures related to aggregation have been estimated on the basis of the reference hypernetted chain approximation for the pair correlation function.

**3.1.2 Percolation and related dynamics.** By further decreasing the temperature within the low and medium density region, the small clusters characterizing the polymerized state start to connect into large clusters that span the whole system. The parameter range of the resulting low-temperature state is indicated by region III in Fig. 4. The two snapshots shown in Fig. 5 illustrate the change of microstructure between region II and III. If one cluster connects two opposite ends of the simulation cell we consider the system as percolated.

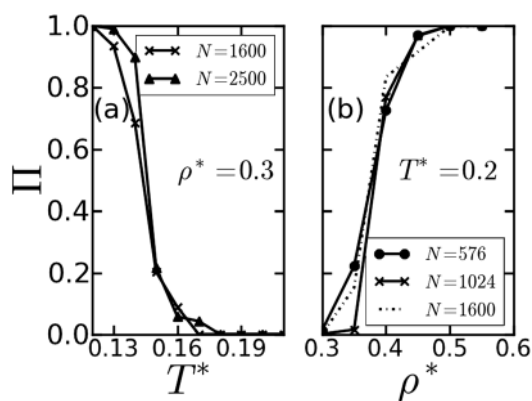
In order to determine the percolation transition more quantitatively, we plot in Fig. 6(a) the percolation probability  $\Pi$  at the density  $\rho^* = 0.3$  for two different system sizes as function of the temperature  $T^*$ . In principle, the transition temperature is determined by the crossing point of the curves for different system sizes. However, to restrict the computational effort we limit the system size to  $N = 1024$  at  $\rho^* > 0.2$  and  $N = 576$  at  $\rho^* < 0.2$ . For these systems, we determine the transition temperatures by the point where  $\Pi(T^*) \sim 0.5$  (see, *e.g.*, ref. 43 for a similar strategy). Nevertheless, as seen from Fig. 6(a), rather large system sizes ( $N = 1024$ –2500) are required to identify the percolation temperature from the plots of  $\Pi(T^*)$ ; for smaller sizes ( $N = 576, 1024$ ) the data are plagued by pronounced statistical errors. Indeed, from the perspective of reducing finite-size effects it turns out to be advantageous to consider the percolation probability as function of the density (rather than as function of  $T^*$ ). Corresponding data are plotted in Fig. 6(b). By increasing



**Fig. 4** Phase diagram of the system at low and medium densities. Regions I, II and III correspond to the homogeneous fluid (I), the string fluid (II), and the percolated fluid (III), respectively. The upper (lower) line denotes the temperatures  $T^*(\rho^*)$  related to the polymerization (percolation).



**Fig. 5** DMD simulation snapshots of the system at  $\rho^* = 0.1$  at two temperatures close to the percolation transition occurring at  $T_{\text{perc}}^* = 0.134$ . In (a) the system is close above the transition ( $T^* = 0.15$ ) while in (b) it is close below the percolation threshold ( $T^* = 0.125$ ).



**Fig. 6** (a) Percolation probability  $\Pi$  as function of the temperature at  $\rho^* = 0.3$  for two different system sizes. (b) Percolation probability as function of the density  $\rho^*$  at temperature  $T^* = 0.2$ .

the density the percolation temperature continuously increases. Finally, at the density  $\rho^* \sim 0.55$  the polymerization and the percolation lines collapse.

We now turn to the question whether the percolation (and accompanying network formation) in our system leads to gelation. Indeed, previous studies of a variety of aggregating colloidal systems<sup>21</sup> have shown that percolation is *prerequisite* of

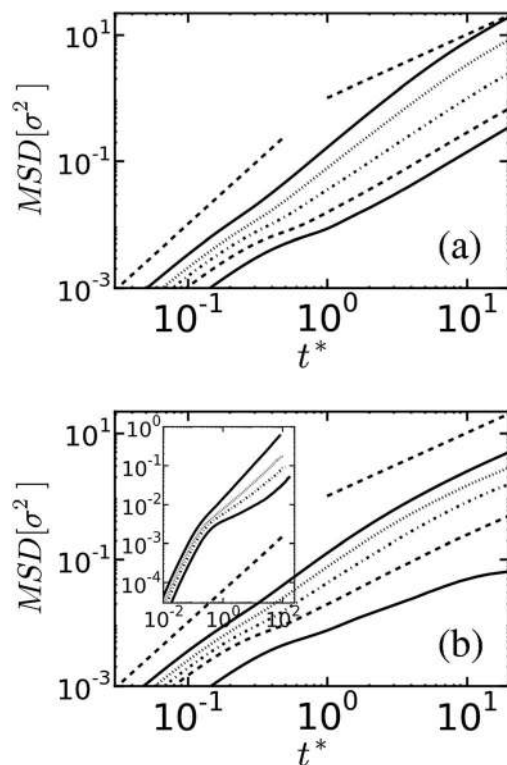
gelation, however, it is not sufficient. A gel or glass is characterized by transient networks that change the dynamic properties of the system. Due to the network structure the motion of the particles slows down significantly. Network formation can become enhanced in systems with long-ranged particle interactions; such systems are therefore more likely to build gel phases.<sup>43</sup> Another factor that favors gelation is branching. Recent studies of systems of dipolar dumbbells have shown that even a modest elongation of the particles leads to branching and, at very low temperatures, to gelation.<sup>22,43</sup> Since our model allows the charges within the colloidal particles to fluctuate, the particles have some similarities with dumbbells, and branching may occur more likely than in point-dipole systems.

As an important indicator of anomalous dynamical behavior within the percolated phase we determine the mean-squared displacement (MSD), defined by

$$\Delta r^2(t) = \left\langle \frac{1}{N} \sum_{i=1}^N [r_i(t) - r_i(0)]^2 \right\rangle. \quad (5)$$

In gel-like systems the MSD shows a plateau at intermediate times between the ballistic and diffusive regime.<sup>17</sup> This slowing-down mechanism can be explained by particles trapped in transient networks.

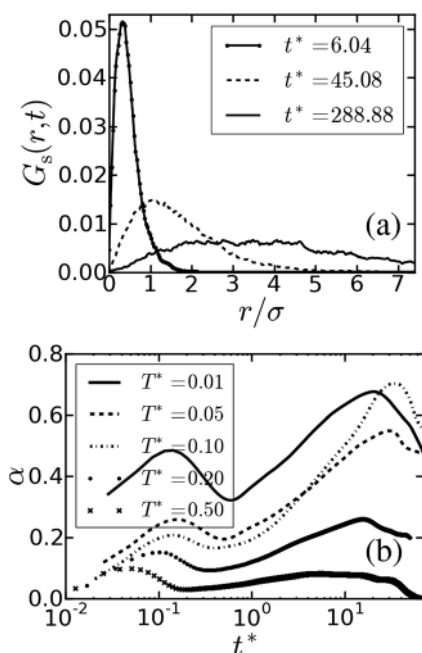
In Fig. 7 we plot the MSD of our system at  $\rho^* = 0.1$  and  $\rho^* = 0.5$  at different temperatures in a double-logarithmic



**Fig. 7** The MSD defined according to eqn (5) at (a)  $\rho^* = 0.1$  and (b)  $\rho^* = 0.5$  in a double-logarithmic representation. The lines correspond to different temperatures  $T^* = 0.3, 0.25, 0.20, 0.10, 0.05$  from top to bottom. The dashed lines show ideal ballistic (slope 1) and diffusive (slope 2) behavior. The inset of (b) shows the MSD at  $\rho^* = 0.5$  at larger time scales for the temperatures  $T^* = 0.2, 0.15, 0.10, 0.05$  (from top to bottom).

representation. At small times all systems show regular ballistic behavior characterized by  $\Delta r^2(t) \propto t^2$ . At very high temperatures ( $T^* > 0.3$ ) this ballistic behavior changes directly into diffusive behavior  $\Delta r^2(t) \propto t$ . At lower temperatures we observe (for both densities) deviations from this simple behavior, as seen in Fig. 7 (a) and (b). Specifically, the MSD of the dilute system [see Fig. 7 (a)] displays a time-dependence with exponent less than one at intermediate times ( $t^* \sim 0.1$ –1) for all temperatures  $T^* < 0.25$ . This implies that already the string formation occurring below the polymerization ( $T_{\text{poly}}^* = 0.247$ ) somewhat slows down the dynamics. An even more pronounced slowing-down is seen at the temperatures  $T^* = 0.10$  and  $T^* = 0.05$ , where the system is within the percolated phase ( $T_{\text{perc}}^* = 0.137$ ). At the medium density  $\rho^* = 0.5$  the effects in the afore-mentioned temperature range are less pronounced. However, by further cooling the denser system towards  $T^* = 0.05$  we again observe a pronounced plateau in the MSD. This is even better revealed by the inset of Fig. 7(b). The time range related to the trapping of the particles is almost two orders of magnitude larger than in the low-density case ( $\rho^* = 0.1$ ). Only at very long times the particles can escape their cages, yielding eventually a diffusive regime. Another interesting point concerns the “cage size”, that is, the typical length related to the plateau in the MSD. As seen from Fig. 7(b) [and, less clearly, also from Fig. 7(a)], this length is significantly smaller than one particle diameter. Such small cage size is reminiscent of what one finds in various polymeric,<sup>44</sup> dipolar,<sup>45</sup> and glass-forming<sup>44</sup> systems. On the other hand, much larger cage sizes of the order of one particle diameter are observed in typical colloidal gels.<sup>43,46</sup>

The appearance of transient networks in our system is also reflected by the self-part of the van Hove function,<sup>47</sup>  $G_s(r, t)$ . In a purely diffusive or ballistic system,  $G_s(r, t)$  is a gaussian function. Results for  $G_s(r, t)$  are plotted in Fig. 8(a), where we



**Fig. 8** (a) Self part of the van Hove function  $G_s(r, t)$  as function of the distance and three times  $t^*$  at  $\rho^* = 0.1$  and  $T^* = 0.01$ . (b) Non-gaussian parameter  $\alpha(t)$  as function of the time at density  $\rho^* = 0.1$  and different temperatures.

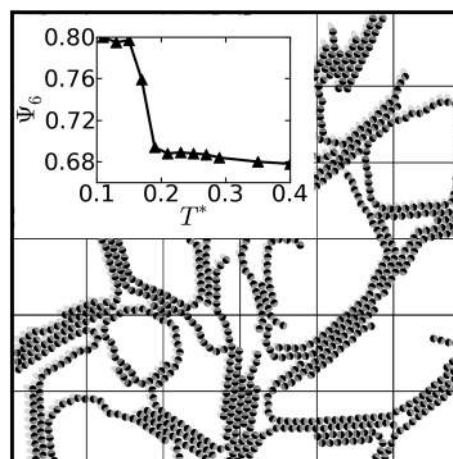
consider three typical times at  $\rho^* = 0.1$ . Deviations from the standard gaussian behavior are seen particularly at the small time  $t^* \sim 6$  and intermediate time  $t^* \sim 45$ . In order to quantify these deviations we determine the parameter  $\alpha$  defined by

$$\alpha(t) = \frac{\langle (\Delta r(t))^4 \rangle}{3 \langle (\Delta r(t))^2 \rangle^2} - 1. \quad (6)$$

The function  $\alpha(t)$  is zero in both, the ballistic and diffusive regime.

In Fig. 8(b) we plot  $\alpha(t)$  at  $\rho^* = 0.1$  and different temperatures. At the highest temperature considered ( $T^* = 0.5$ ) the  $\alpha$  parameter is very small, indicating that the van Hove function is nearly gaussian at all times. Decreasing the temperature leads to an emergence of two peaks at small and large times. The peak at large times becomes particularly pronounced right below the percolation transition which takes place at  $T_{\text{perc}}^* = 0.137$ . In various recent simulation studies of aggregating systems,<sup>43,48</sup> such peaks in  $\alpha(t)$  have been interpreted as presence of different “populations” of particles (*i.e.* as dynamic heterogeneities). As an attempt to identify such populations in the present system, we have calculated the distribution of squared displacements,<sup>49</sup>  $P(r^2, t)$ . However, we did not find any significant behavior (such as a double-peak structure indicating presence of “slow” and “fast” particles) at the conditions considered.

To summarize our discussion about the appearance of gelation in the present (model) system, we note that there are some features pointing in this direction, whereas other are not. One main feature typical for gels is the presence of percolated and branched structures as seen in Fig. 5(b) [and also later in Fig. 9]. Moreover, particularly at intermediate densities we find that these structures lead to plateau-like behavior of the mean-squared displacement, accompanied by a peak of the alpha-parameter. However, the typical cage size of a gel is not observed in our system. Also, there is no evidence for dynamical heterogeneities, and the observed structures are transient rather than stable (as it is the case, *e.g.*, in gels of branched dendrimers). We therefore consider the present model involving short-ranged, fluctuating dipolar interactions as a system showing dynamic anomalies with weak hints pointing into a gel-like behavior.



**Fig. 9** Snapshot at  $\rho^* = 0.3$  and  $T^* = 0.13$  (within the percolated phase). The inset shows the order parameter  $\Psi_6$  as function of  $T^*$ .

### 3.2 Ordered phases

At low temperatures and sufficiently high densities the dipole-like colloids start to build crystalline structures characterized by long-ranged positional ordering of the particles. The degree of translational order can be studied by various bond-order parameters. Here we focus on the hexagonal order parameter<sup>50</sup>

$$\Psi_6 = \left\langle \frac{1}{N_b} \left| \sum_{i=1}^{N_b} \exp(i6\theta_{ij}) \right| \right\rangle, \quad (7)$$

where  $N_b$  is the number of neighbours, and  $\theta_{ij}$  denotes the angle of the bond vector  $\mathbf{r}_{ij}$  between neighbouring particles  $i$  and  $j$  relative to a fixed, but arbitrary, direction. We consider particles as neighbours if their distance is smaller than the distance related to the first minimum of the in-plane pair correlation function  $g(r)$ . If each particle is surrounded by six nearest neighbours the order parameter  $\Psi_6$  becomes one (hexagonal lattice (HL)), whereas in a homogeneous state  $\Psi_6$  is zero.

In addition to positional order, the degree and type of global orientational order (if it occurs) is also of interest. To this end we introduce the ordering matrix<sup>51</sup>

$$\mathbf{Q} = \frac{1}{2N} \sum_{i=1}^N (3\hat{\boldsymbol{\mu}}_i \hat{\boldsymbol{\mu}}_i - \mathbf{I}). \quad (8)$$

In eqn (8),  $\hat{\boldsymbol{\mu}}_i$  corresponds to the unit vector of the orientation of particle  $i$ , and  $\mathbf{I}$  is the unity matrix. The global director  $\hat{\mathbf{d}}$  is obtained by normalizing the eigenvector corresponding to the largest eigenvalue of the matrix  $\mathbf{Q}$ . The first-rank orientational order parameter is then defined by

$$P_1 = \left| \frac{1}{N} \sum_{i=1}^N \hat{\boldsymbol{\mu}}_i \cdot \hat{\mathbf{d}} \right|, \quad (9)$$

which is unity in a ferroelectric state and zero in an anti-ferroelectric or isotropic phase. The second-rank order parameter  $P_2$  is defined as the largest eigenvalue of  $\mathbf{Q}$ , and describes the alignment of the particles without carrying the information of the direction. As we will show below, the present system has (only) a ferroelectric phase. Hence, we focus on the order parameter  $P_1$ .

The transition into a ferroelectric state is characterized by an increase of the parameter  $P_1$  from zero to one. The corresponding curves  $P_1(T^*)$  turned out to be essentially independent of the system size (presumably due to the short-ranged character of the pair interactions in our model). We thus determine the ferroelectric transition from simulations with  $N = 1024$ . In addition to the system size, we investigate the impact of the geometry of the simulation box. To this end we implemented a variable box-length Monte-Carlo algorithm.<sup>52</sup> To preserve a canonical ensemble, the area of the simulation box was kept constant. We also performed a few simulations with a fixed, rectangular shape of the simulation box. However, the order parameter turned out to be robust against all these tests.

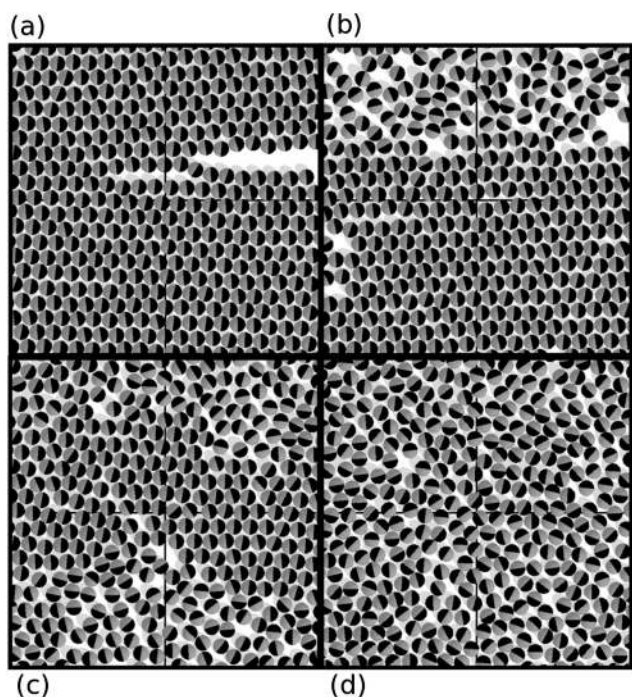
**3.2.1 Low densities.** As discussed in Sec. 3.1, the regime of low and medium densities is characterized by a polymerization and percolation transition. To complete the picture, we now discuss the corresponding behavior of the orientational and translational order parameters [see eqn (7) and (9)]. As an example we consider the density  $\rho^* = 0.3$ . In Fig. 9, we present

a snapshot illustrating the structure of the system at temperature  $T^* = 0.13$ , which is slightly below the percolation temperature (see Fig. 4). As expected, one observes system-spanning clusters consisting of dipolar chains. Interestingly, however, some of these chains are merged into “bundles” characterized by a parallel arrangement of pieces of chains. Within these bundles, neighbouring chains are shifted relative to one another by half a particle diameter. These arrangements correspond to an energetically highly favorable situation, as reflected by the sketch in the last row in Fig. 2. Having in mind that the present colloidal particles lack of any isotropic attractive interactions, we conclude that the bundle formation observed in Fig. 9 is driven by the attractive, lateral interactions between (pieces of) dipolar chains. It is clear that these lateral interactions and the resulting bundles also favor branching and thus, gel-like behavior, as reflected *e.g.* by the MSD (see Fig. 7(b)). A further consequence of the pronounced local ordering is that the bundle structures (such as those in Fig. 9 for  $\rho^* = 0.3$ ) are characterized by relatively large values of the hexagonal order parameter,  $\Psi_6$ . The temperature dependence of  $\Psi_6$  is plotted in the inset of Fig. 9. From the inflection point of  $\Psi_6$  we can determine a hexagonal transition temperature at  $T_{\text{hex}}^* = 0.174$ , which is slightly higher than the percolation temperature  $T_{\text{perc}}^* = 0.161$ . We note, however, that the system at temperatures  $T^* < T_{\text{hex}}^*$  is not a solid; rather it remains to be disordered down to the lowest temperature considered. Also, there is (obviously) no global orientational order, that is,  $P_1 \sim 0$ . Similar behavior of  $\Psi_6$  and  $P_1$  is found at other densities in the range  $\rho^* < 0.4$ .

We note that bundle formation has also been observed in 2D systems of dipolar particles with additional Yukawa interaction<sup>53</sup> where, however, the density was higher and. In fact, our model prefers bundle formation as compared to a system of true dipolar spheres, where the chain-chain interaction is considerably weaker. This becomes clear from Fig. 2 (bottom), where we compare the energy of hexagonal-like configurations in the two types of models. As a consequence, our model supports bundle formation already at lower densities. Prominent *real* systems where pronounced bundling and accompanying local hexagonal order occurs, are ferro-colloids in external magnetic fields,<sup>54</sup> but also polarizable colloids<sup>26</sup> and Janus colloids<sup>55</sup> in electric fields.

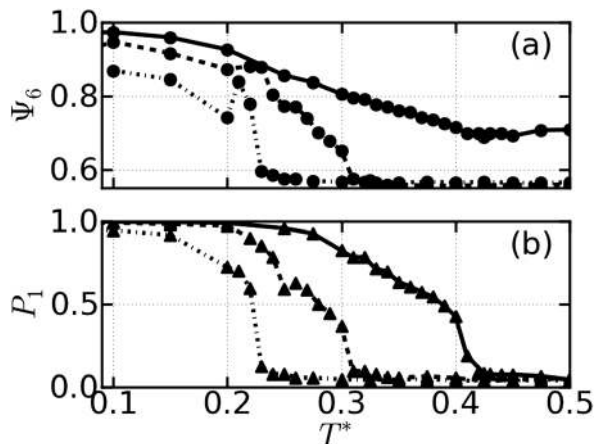
**3.2.2 High densities.** In the density range discussed so far, hexagonal ordering occurs only locally (*i.e.*, within bundles). This changes at densities  $\rho^* \geq 0.6$  where we find, at sufficiently low temperatures, the formation of crystalline structures characterized by long-range positional, hexagonal order. The change from the isotropic high-temperature into the hexagonal low-temperature state is illustrated in Fig. 10, where we present various snapshots of systems at the representative density  $\rho^* = 0.9$ . At the lowest temperature considered, the system is nearly close-packed apart from small defects.

The hexagonal translational structure is, in fact, expected in view of the behavior of the pure HS system underlying our model. Note, however, that the HS systems freezes only at a density<sup>56</sup>  $\rho^* \approx 0.91$ , that is, much later than the present system. This is consistent with our findings in the previous paragraph, according to which the dipole-like interactions tend to stabilize the hexagonal-like ordering at lower densities (as compared to HS).



**Fig. 10** Snapshots at  $\rho^* = 0.9$  at different temperatures illustrating the melting transition. The reduced temperature is  $T^* = 0.2$  in (a),  $T^* = 0.3$  in (b),  $T^* = 0.4$  in (c) and  $T^* = 0.5$  in (d).

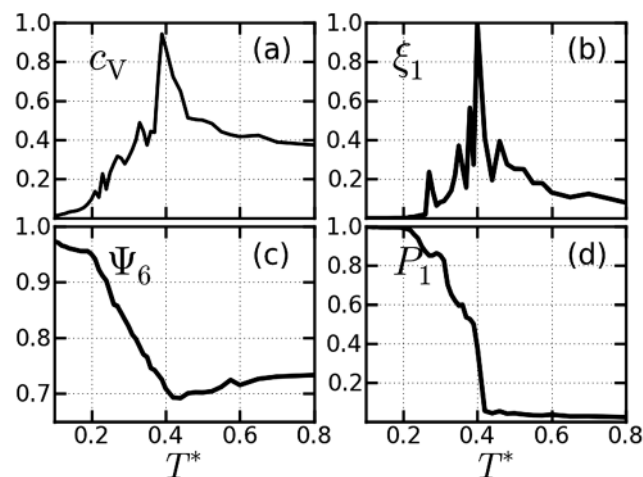
A further, and much more dramatic, consequence of the dipole-like interactions is that the translational ordering at high densities is accompanied by long-ranged ferroelectric order. This can be directly seen from the (low-temperature-) snapshot in Fig. 10(a) and 10(b), and, more quantitatively, from the behavior of the parameters  $\Psi_6$  and  $P_1$ . In Fig. 11 we have plotted the functions  $\Psi_6(T^*)$  and  $P_1(T^*)$  for three (large) values of  $\rho^*$ . In all cases, one observes a sudden, pronounced increase of  $P_1$  upon lowering the temperature from the isotropic high-temperature state ( $P_1 \sim 0.0$ ). Moreover, the temperature where  $P_1$  starts to deviate from zero, coincides with the temperature where the parameter  $\Psi_6$  increases significantly from the smaller (and essentially  $T^*$ -independent) values characterizing the high-



**Fig. 11** (a) Order parameters  $\Psi_6$  and (b)  $P_1$  at densities  $\rho^* = 0.9$  (straight line), 0.8 (dashed line) and 0.6 (dotted line).

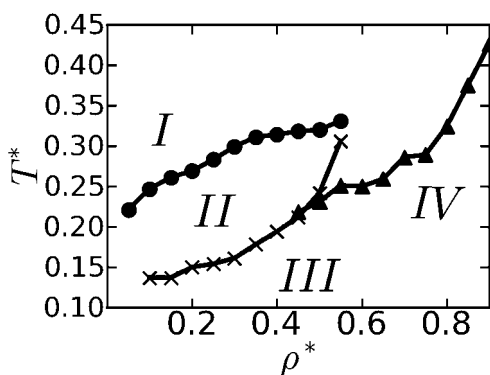
temperature state. In fact, the data in Fig. 11 suggest that the order parameters increase from their high- $T^*$  values nearly continuously, indicating presence of a second-order (or, at the least, weak first-order) phase transition. Here, we did not attempt to clarify that issue systematically. We note, however, that the coupled hexagonal/ferroelectric transition is accompanied by significant fluctuations. This is illustrated in Fig. 12, where we plot the functions  $\Psi_6(T^*)$  and  $P_1(T^*)$  together with the specific heat  $c_V$  (measuring fluctuations of the (potential) energy), and the quantity  $\xi_1 = \langle P_1^2 \rangle - \langle P_1 \rangle^2$  (the latter has been normalized by its maximum value since the absolute values are rather small). Both quantities display a pronounced peak at the temperature related to the onset of the hexagonal/ferroelectric ordering. Similar behavior is found at other values of  $\rho^*$  in the high-density regime, with the peak heights in  $c_V$  and  $\xi_1$  becoming less pronounced, the smaller  $\rho^*$ .

The appearance of long-ranged ferroelectric order in our model is in marked contrast to what is known about the behavior of true dipolar spheres in 2D. In fact, while model systems like dipolar hard and soft spheres do display ferroelectric order in the 3D case, MC simulations of corresponding 2D systems rather reveal frustrated structures characterized by large domains of *local* ferroelectric order, but no long-range order.<sup>57</sup> The same conclusion emerged from (MD) simulations of confined, slab-like dipolar systems where the long-ranged ordering is lost upon lowering the film thickness towards the 2D limit.<sup>58</sup> Clearly, an important technical issue particularly at very high densities and low temperatures concerns the influence of the system size considered in the simulations. Indeed, for true dipolar systems it is well known that a too small simulations system can stabilize ferroelectric ordering under conditions, where simulations with larger systems would just reveal large domains. To check this point, we have additionally run some simulations with  $N = 2000$ – $4000$  particles. Additionally we have investigated the decay behavior of the two particle correlation function of the dipolar vectors, that is, the function  $g_{110}(r) = \langle \sum_i \sum_{j \neq i} \delta(r - r_{ij}) \hat{\mu}_i \hat{\mu}_j \rangle / (N\rho)$ , where  $\hat{\mu}_i$  is a unit



**Fig. 12** Transition from isotropic fluid to ordered phase at density  $\rho^* = 0.9$ . In (a) we plot the specific heat  $c_V$ , in (b) the fluctuations of the orientational order  $\xi_1$ . The order parameters at the transition are shown in (c)  $\Psi_6$  and (d)  $P_1$ .





**Fig. 13** Phase diagram involving all transition lines determined in this paper. The labels *I*, *II*, *III*, and *IV* refer to the isotropic fluid, the polymerized fluid, the percolated phase, and the ferroelectric crystal, respectively. We have not attempted to determine the transition between percolated fluid and the crystal at low temperatures.

vector. In the limit of large  $r$ , this function should saturate to a finite value determined by the order parameter  $P_1$ .<sup>59</sup> In our case, for systems of  $N = 1500$ , the function  $g_{110}(r)$  still revealed additional peaks of the correlation function at half length of the simulation box. For a system size of  $N = 2500$  these peaks disappear. The system size of  $N \sim 2500$  is thus sufficient to check for true long-range ferroelectric order. Inspecting snapshots, it turns out that the larger systems generally display more defects. However, on the whole the combined hexagonal and ferroelectric ordering remains.

#### 4 Conclusion

We have used DMD computer simulations to study a system of nano-particles with dipole-like interactions in two dimensions. A prerequisite of the DMD technique (and the main reason for its computational efficiency), are discontinuous, short-ranged potentials. To this end we have approximated the true dipole-dipole interaction by a short-ranged three-step potential suggested in an earlier study of a corresponding 3D system.<sup>23</sup> Based on that model, which mimics the directional dependence of the dipolar interactions on short length scales, we were able to study a wide range of densities and temperatures. An overview of the equilibrium behavior, that is, a rough (yet not complete) phase diagram, is given in Fig. 13. Apart from a homogeneous, isotropic high-temperature phase (I), we find a polymerized (“string”) fluid (II), a percolated phase (III), and a hexagonal, ferroelectric crystal (IV). An open point, which was beyond the scope of the present study, concerns the transition between the percolated and the crystal phase, as well as the occurrence of glassy phases. We also note that we have seen no evidence for a gas-liquid transition within the fluid phase, consistent with the behavior of the corresponding 3D model<sup>23</sup> and also with that of true dipolar hard or soft spheres in two and three dimensions.<sup>14,15</sup> On the other hand, the absence of gas-liquid condensation is in contrast to many other aggregating systems such as, *e.g.* Janus particles, which display a combined condensation-micellisation transition.<sup>60</sup> Similar models with short-ranged potentials, such as patchy particles, also show a gas-liquid separation provided the number of patches per particle is sufficient.<sup>16,61</sup>

As described in the previous sections, all lines in Fig. 13 have been defined *via* a thorough analysis of suitable order parameters. In particular, to define the polymerization line we used the so-called degree of polymerization (measuring the number of particles involved in clusters), which showed almost no finite-size effects (contrary to the specific heat). Interestingly, the resulting line agrees quite well with a corresponding result from a recent integral equation study of 2D systems of true dipoles.<sup>18</sup> Moreover, our polymerization temperatures are very close to those found in the 3D version of the present model,<sup>23</sup> although the latter (DMD) study used a somewhat different order parameter, namely a strong increase of the average cluster size. Less agreement is found with respect to the percolation which occurs in both, the 3D<sup>23</sup> and the 2D system, at temperatures below the polymerization. We have located the percolation threshold in the “traditional” way, that is, by monitoring the percolation probability. The resulting percolation temperatures are significantly lower than those in the 3D model. We note however, that ref. 23 used a different definition of percolation such that the quantitative comparison with our data has to be considered with care. We would like to note that in the case of true dipoles in 2D ring formation is observed in the polymerized fluid phase,<sup>62</sup> contrary to the 3D case, where this effect is less pronounced. A similar system where such a behavior can be observed is a mixture of patchy particles, with 2 and 3 patches. In these systems rings and inter-cluster bonding is also very pronounced, which is due to particles with 3 patches building connections.<sup>63</sup> In our system, however, the formation of rings is relatively weak in the polymerized fluid phase.

Given the preference of head-to-tail configurations and thus, chain formation, in our model, the very appearance of polymerization and percolation at low temperatures and densities is clearly expected. A less explored question concerns the corresponding dynamics. While systems of true dipolar hard or soft spheres (in zero field) display normal dynamics despite pronounced chain formation,<sup>45</sup> a recent MD study of dipolar dumbbells<sup>43</sup> revealed anomalous, gel-like dynamics accompanying the formation of branched chains and networks. Our model bears some similarity with the dumbbells insofar as the “dipoles” in our particles consist of two “charges” whose position can fluctuate. Motivated by this fact we have investigated the present system *via* various time-dependent (single-particle) quantities. For some state points deep within the percolated phase, we do indeed find features reminiscent of gels such as plateau-like behavior of the mean-squared displacement, accompanied by a peak of the alpha-parameter. The picture emerging from these measures (and from a corresponding structural analysis) is that the particles form transient networks consisting of percolated chains and bundles thereof. Of course, network formation also occurs in systems of true dipoles,<sup>15</sup> including the dipolar dumbbells studied in ref. 43. However, compared to the dumbbells it seems that the networks in our case are less stable. One factor might be that the interactions in ref. 43 are of coulombic and thus, long-ranged nature, a factor which tends to stabilize the networks. Concerning the dynamics, we note that the present system shows no evidence of dynamical heterogeneities, and that the cage sizes extractable from the MSD are extremely small. Taken altogether, we conclude that the dynamics do possess anomalous features, but that there is no clear

gel “phase” such as in systems of dipolar dumbbells<sup>43</sup> and patchy particles.<sup>17,46</sup>

Finally, we have investigated the crystallization. As expected in view of the 2D character of our model, the particles form a hexagonal lattice. Interestingly, these solid-like structures appear already at densities far below the freezing density of the corresponding hard disk fluid. Moreover, the ordering into a hexagonal lattice goes together with the onset of long-ranged ferroelectric order. In this respect, our model behaves fundamentally different from 2D systems of true dipolar (hard or soft) spheres where, at the most, large ferroelectric domains (rather than true global polarization) are observed. In our view, the main reason for this difference is that the present model slightly prefers (relative to the true dipolar case) arrangements of parallel oriented, shifted chains.

Taken altogether, our study reveals a complex static and dynamic behavior of the colloidal model system under consideration. Clearly, the short-ranged nature of our model is an approximation, when one thinks about true dipoles; we note however, that in a true colloidal system involving particles with charges, the *effective* range of the interaction can be tuned by parameters such as salt, pH, or concentrations of ionic adsorbing species. From our view, one particularly interesting (and novel) result is the gel-like behavior found in the percolated phase. Indeed, the unusual dynamics observed, *e.g.*, in the mean-squared displacement (see Fig. 7) suggests a non-trivial, non-linear behavior also in rheological properties such as the shear viscosity and, more generally, the mechanical response of the material to external stress. This is clearly an aspect which deserves further attention and could also be studied *via* the DMD method. Moreover, given the overwhelming variety of colloidal particles being synthesized with increasing complexity and precision,<sup>64</sup> it would be very interesting to extend the present study towards more complex particles which have, *e.g.*, quadrupolar character.<sup>27</sup> Work in these directions is in progress.

## Acknowledgements

We gratefully acknowledge financial support from the Deutsche Forschungsgemeinschaft through the International Research Training Group 1524 “ Self-Assembled Soft Matter Nano-Structures at Interfaces” (project C 3.1). CH and OV acknowledge partial support for this research provided by the US-NSF’s Research Triangle MRSEC (DMR-1121107).

## References

- 1 M. Parthasarathy and D. J. Klingenberg, *Mater. Sci. Eng., R*, 1996, **17**, 57–103.
- 2 S. C. Glotzer and M. J. Solomon, *Nat. Mater.*, 2007, **6**, 557–562.
- 3 A. van Blaaderen, *Nature*, 2006, **439**, 545–546.
- 4 Z. L. Zhang and S. C. Glotzer, *Nano Lett.*, 2004, **4**, 1407–1413.
- 5 F. Romano, P. Tartaglia and F. Sciortino, *J. Phys.: Condens. Matter*, 2007, **19**, 322101.
- 6 A. Walther and A. H. E. Müller, *Soft Matter*, 2008, **4**, 663–668.
- 7 P. Y. Keng, I. Shim, B. D. Korth, J. F. Douglas and J. Pyun, *ACS Nano*, 2007, **1**, 279–292.
- 8 A. Perro, S. Reculosa, S. Ravaine, E. Bourgeat-Lami and E. Duguet, *J. Mater. Chem.*, 2005, **15**, 3745–3760.
- 9 Q. Chen, J. K. Whitmer, S. Jiang, S. C. Bae, E. Luijten and S. Granick, *Science*, 2011, **331**, 199–202.
- 10 J. R. Millman, K. H. Bhatt, B. G. Prevo and O. D. Velev, *Nat. Mater.*, 2005, **4**, 98–102.
- 11 K. H. Bhatt and O. D. Velev, *Langmuir*, 2004, **20**, 467–476.
- 12 J. J. Benkoski, R. M. Deacon, H. B. Land, L. M. Baird, J. L. Breidenich, R. Srinivasan, G. V. Clatterbaugh, P. Y. Keng and J. Pyun, *Soft Matter*, 2010, **6**, 602–609.
- 13 D. Wei and G. N. Patey, *Phys. Rev. Lett.*, 1992, **68**, 2043–2045.
- 14 J. J. Weis and D. Levesque, *Phys. Rev. Lett.*, 1993, **71**, 2729–2732.
- 15 J. M. Tavares, J. J. Weis and M. M. Telo da Gama, *Phys. Rev. E*, 2006, **73**, 041507.
- 16 E. Bianchi, J. Largo, P. Tartaglia, E. Zaccarelli and F. Sciortino, *Phys. Rev. Lett.*, 2006, **97**, 168301.
- 17 C. Mayer, F. Sciortino, P. Tartaglia and E. Zaccarelli, *J. Phys.: Condens. Matter*, 2010, **22**, 104110.
- 18 L. Luo and S. H. L. Klapp, *J. Chem. Phys.*, 2009, **131**, 034709.
- 19 F. Sciortino, A. Giacometti and G. Pastore, *Phys. Rev. Lett.*, 2009, **103**, 237801.
- 20 J. M. Tavares, J. J. Weis and M. M. Telo da Gama, *Phys. Rev. E*, 2002, **65**, 061201.
- 21 E. Zaccarelli, *J. Phys.: Condens. Matter*, 2007, **19**, 323101.
- 22 R. Blaak, M. A. Miller and J.-P. Hansen, *Europhys. Lett.*, 2007, **78**, 26002.
- 23 A. Goyal, C. K. Hall and O. D. Velev, *Phys. Rev. E*, 2008, **77**, 031401.
- 24 B. J. Alder and T. E. Wainwright, *J. Chem. Phys.*, 1959, **31**, 459–466.
- 25 H. S. Gulati and C. K. Hall, *J. Chem. Phys.*, 1997, **107**, 3930–3946.
- 26 S. O. Lumsdon, E. W. Kaler and O. D. Velev, *Langmuir*, 2004, **20**, 2108–2116.
- 27 S. Gangwal, A. Pawar, I. Kretschmar and O. D. Velev, *Soft Matter*, 2010, **6**, 1413–1418.
- 28 A. Goyal, C. K. Hall and O. D. Velev, *J. Chem. Phys.*, 2010, **133**, 064511.
- 29 N. Osterman, D. Babič, I. Poberaj, J. Dobnikar and P. Zihlerl, *Phys. Rev. Lett.*, 2007, **99**, 248301.
- 30 J. J. Jurez and M. A. Bevan, *J. Chem. Phys.*, 2009, **131**, 134704.
- 31 O. D. Velev and S. Gupta, *Adv. Mater.*, 2009, **21**, 1897–1905.
- 32 S. H. Klapp, *Mol. Simul.*, 2006, **32**, 609–621.
- 33 C. Alvarez, M. Mazars and J.-J. Weis, *Phys. Rev. E*, 2008, **77**, 051501.
- 34 H. Schmidle and S. H. L. Klapp, *J. Chem. Phys.*, 2011, **134**, 114903.
- 35 D. C. Rapaport, *J. Chem. Phys.*, 1979, **71**, 3299–3303.
- 36 A. Bellemans, A. Oraban and D. Van Belle, *Mol. Phys.*, 1980, **39**, 781.
- 37 H. C. Andersen, *J. Chem. Phys.*, 1980, **72**, 2384–2393.
- 38 Y. Zhou, C. K. Hall and G. Stell, *J. Chem. Phys.*, 1995, **103**, 2688–2695.
- 39 Y. Zhou, M. Karplus, J. M. Wichert and C. K. Hall, *J. Chem. Phys.*, 1997, **107**, 10691–10708.
- 40 G. P. Johari, E. Tombari, S. Presto and G. Salvetti, *J. Chem. Phys.*, 2002, **117**, 5086–5091.
- 41 S. S. Das, A. P. Andrews and S. C. Greer, *J. Chem. Phys.*, 1995, **102**, 2951–2959.
- 42 J. Stambaugh, K. Van Workum, J. F. Douglas and W. Losert, *Phys. Rev. E*, 2005, **72**, 031301.
- 43 M. A. Miller, R. Blaak, C. N. Lumb and J.-P. Hansen, *J. Chem. Phys.*, 2009, **130**, 114507.
- 44 J. Baschnagel, C. Bennemann, W. Paul and K. Binder, *J. Phys.: Condens. Matter*, 2000, **12**, 6365.
- 45 J. Jordanovic, S. Jäger and S. H. L. Klapp, *Phys. Rev. Lett.*, 2011, **106**, 038301.
- 46 J. Russo, P. Tartaglia and F. Sciortino, *J. Chem. Phys.*, 2009, **131**, 014504.
- 47 J.-P. Hansen and J. R. McDonald, *Theory of simple Liquids*, Academic Press, 2006.
- 48 S. C. Glotzer, *J. Non-Cryst. Solids*, 2000, **274**, 342–355.
- 49 A. M. Puertas, M. Fuchs and M. E. Cates, *J. Chem. Phys.*, 2004, **121**, 2813–2822.
- 50 J. R. Errington, P. G. Debenedetti and S. Torquato, *J. Chem. Phys.*, 2003, **118**, 2256–2263.
- 51 M. P. Allen and D. J. Tildesley, *Computer Simulations of Liquids*, Oxford University Press, 1986.
- 52 A. J. Schultz, C. K. Hall and J. Genzer, *J. Chem. Phys.*, 2004, **120**, 2049–2055.
- 53 J.-J. Weis, *J. Phys.: Condens. Matter*, 2003, **15**, S1471.
- 54 D. Heinrich, A. R. Goñi, A. Smessaert, S. H. L. Klapp, L. M. C. Cerioni, T. M. Osán, D. J. Pusiol and C. Thomsen, *Phys. Rev. Lett.*, 2011, **106**, 208301.
- 55 S. Gangwal, O. J. Cayre and O. D. Velev, *Langmuir*, 2008, **24**, 13312–13320.
- 56 A. Jaster, *Phys. Rev. E*, 1999, **59**, 2594–2602.
- 57 J. J. Weis, *Mol. Phys.*, 2002, **100**, 579.

- 
- 58 R. A. Trasca and S. H. L. Klapp, *J. Chem. Phys.*, 2008, **129**, 084702.  
59 J. J. Weis and D. Levesque, *Phys. Rev. E*, 1993, **48**, 3728–3740.  
60 F. Sciortino, A. Giacometti and G. Pastore, *Phys. Rev. Lett.*, 2009, **103**, 237801.  
61 E. Bianchi, P. Tartaglia, E. Zaccarelli and F. Sciortino, *J. Chem. Phys.*, 2008, **128**, 144504.  
62 E. Lomba, F. Lado and J. J. Weis, *Phys. Rev. E*, 2000, **61**, 3838–3849.  
63 P. Tartaglia and F. Sciortino, *J. Phys.: Condens. Matter*, 2010, **22**, 104108.  
64 I. Kretzschmar and J. H. K. Song, *Curr. Opin. Colloid Interface Sci.*, 2011, **16**, 84–95.